Polymer 192 (2020) 122309

Contents lists available at ScienceDirect

Polymer

journal homepage: http://www.elsevier.com/locate/polymer

Anisotropic thermoresponsive hydrogels by mechanical force orientation of clay nanosheets

Lie Chen [a,b], Qingshan Wu [a], Jianqi Zhang [c], Tianyi Zhao [a], Xu Jin [d], Mingjie Liu [a,e,*]

[a] Key Laboratory of Bio-Inspired Smart Interfacial Science and Technology of Ministry of Education, School of Chemistry, Beihang University, Beijing, 100191, PR China
[b] School of Physics, Beihang University, Beijing, 100191, PR China
[c] National Center for Nanoscience and Technology, Beijing, 100190, PR China
[d] Research Institute of Petroleum Exploration and Development, PetroChina, Beijing, 100191, PR China
[e] International Research Institute for Multidisciplinary Science, Beihang University, Beijing, 100191, PR China

ARTICLE INFO

Keywords:
Anisotropic hydrogel
Thermoresponsive nanocomposite
Soft actuator

ABSTRACT

Hydrogels have drawn great attentions in the past two decades due to their excellent biocompatibility and multi stimuli responsiveness, which have a wide range of applications in the field related to tissue engineering, sensor and biomedicine. However, conventional artificial hydrogels are usually isotropic in structure with random crosslinking of polymer chains. To imitate the well-defined hierarchical structures ranging from the molecular scale to macroscopic scale like biological soft tissues in hydrogels. Herein, an anisotropic thermoresponsive hydrogel was reported via a linear remolding of highly stretchable clay-PNIPAm nanocomposite hydrogel by a secondary crosslinking. The as-prepared hydrogel shows anisotropic mechanical performance and can deformed anisotropically in response to temperature change. Besides, the oriented structures of clay nanosheets and polymer network that contribute to understand the anisotropic mechanism of SC-hydrogel was investigated. The special functions of current SC-hydrogel suggest that it may serve as ideal composite gel materials with validity in a variety of applications, such as soft actuators, sensors, and biological materials.

1. Introduction

Hydrogels are three-dimensional polymer networks that contain a large amount of water, known as soft and wet matter, the same as biological soft tissues. They are expected to be promising candidates for biological tissues, such as skeletal muscles and cartilages, etc. [1,2]. However, conventional artificial hydrogels are usually isotropic in structure with random crosslinking of polymer chains. Due to the lack of well-defined hierarchical structures ranging from the molecular scale to macroscopic scale like biological soft tissues, most artificial hydrogels do not show any excellent functions like living bodies do. For example, the skeletal muscle is the core actuation system for driving motion of animal's body, which is achieved using hierarchical principles, triggered by the presence of calcium ions, and produces macroscale contraction from staggered fibrous structures [3,4]. Consequently, introducing sophisticated structures like biological tissues into artificial hydrogels is challenging but promising strategy for the preparation of polymer gels with superb functions.

To date, large varieties of anisotropic hydrogels are developed by researchers all over the world. For example, hydrogels with anisotropic mechanical strength [5–8], swelling ability [9,10], optical properties [11,12], stimuli-responsive deformation [13,14], and anisotropic electrical conductivity [15,16], etc.. Strategies that utilized to prepare these hydrogels including self-assemble under external field (gravity field, shear field, magnetic field, electric field) [17–22], oriented electrospun and prestretching [23,24]. Comparing these strategies, prestretching is rather a simple, and effective method to fabricate anisotropic structure in hydrogels and other soft materials in spite of a stretchable elastic network is a prerequisite.

Learning from nature, having in mind that the well-defined hierarchical, ordered structure is the key prerequisites to fabricate functional hydrogel materials. Herein, a thermoresponsive anisotropic hydrogel is prepared via a linear remolding of highly stretchable clay-PNIPAm nanocomposite hydrogel by a secondary crosslinking. Since the remolded polymer network is locked by the subsequent crosslinking, the resultant hydrogel is anisotropic. The as-prepared secondary crosslinked

* Corresponding author. Key Laboratory of Bio-Inspired Smart Interfacial Science and Technology of Ministry of Education, School of Chemistry, Beihang University, Beijing, 100191, PR China.
E-mail address: liumj@buaa.edu.cn (M. Liu).

https://doi.org/10.1016/j.polymer.2020.122309
Received 14 October 2019; Received in revised form 12 February 2020; Accepted 18 February 2020
Available online 20 February 2020

hydrogel (SC-hydrogel) exhibited birefringence under crossed nicols due to the anisotropic diffraction, revealed the anisotropic microscopic structure inside the SC-hydrogel. The microscopic orientation structure (polymer network and clay nanosheets) endows the SC-hydrogel with macroscopic thermoresponsive anisotropic deformation property. When temperature above the LCST of PNIPAm, the SC-hydrogel shows more than 20% contraction along the stretching direction, the same as the degree of macroscale muscle contraction (varies between approximately 20–40%) [4]. While barely unchanged in its vertical direction. Moreover, the volume change of SC-hydrogel also generates anisotropic contractile stress, which is more than 5 times higher in stretching direction (~5 kPa) than in vertical direction (~1 kPa). The aforementioned characteristics implies that the as-prepared thermoresponsive anisotropic hydrogel closely mimic the natural actuator "skeletal muscle", a tissue specialised to decrease in length when free to move or increase in tension when constrained. Suggest that the SC-hydrogel may serve as ideal composite gel materials in the fields related to soft actuators, sensors, and biological materials.

2. Experimental section

2.1. Materials

All of the following chemical reagents are used as received from Sigma-Aldrich. [*N*-isopropylacrylamide (NIPAm), Acrylamide (AAm), N, N′-Methylenebisacrylamide (BIS), Diethoxyacetophenone (DEOP, Photo-initiator)], clay nanosheets (Laponite XLS, Rockwood), deionized water was obtained via Milli-Q. The photo camera (Cannon 60D) took all photo images in this work. Mercury arc lamp (OSRAM, 500 W) provides ultraviolet light irradiation for the photo-initiated polymerization of the hydrogels. Fluorescence microscope (Nikon, ECLIPSE Ti). CO_2 Laser marking machine (HGTECH, LSC30).

2.2. Preparation of clay-PNIPAm hydrogel

Generally, NIPAm (a sequency of concentration of 1 mol/L, 1.5 mol/L, 2 mol/L, 2.5 mol/L were tested), clay nanosheets (7 wt% ~13 wt% of water amount) and DEOP (1 wt% to monomers) was dissolved in deionized water, then the whole mixture was stirred for 30 min until fully transparent solution was obtained. After 5 min UV irradiation, the clay-PNIPAm hydrogel was prepared.

2.3. Preparation of anisotropic thermoresponsive hydrogel

At first, stretching the as-prepared clay-PNIPAm hydrogel to a certain strain (150%–400%) and fixed on glass slide. Then the prestretched hydrogel was immersed in an aqueous solution of acrylamide (0.5 mol/L, 1 mol/L, 1.5 mol/L, 2 mol/L, 2.5 mol/L), containing BIS (5 wt%, 10 wt%, 15 wt%, 20 wt%, 25 wt%, 30 wt% to monomers) and photo-initiator for certain time. The second network (polyacrylamide) is subsequently synthesized in the presence of first network by UV irradiation for 10 min. The resultant hydrogels are rinsed by ample water to remove residual monomers.

2.4. Characterization

We use environmental scanning electron microscope (QUANTA 250 FEG) to characterize the micro morphology of hydrogel. The as-prepared clay-PNIPAm hydrogel and SC-hydrogel were frozen using low temperature refrigerator for 1 h. Then the hydrogels were freeze dried with freeze drier ((BEKO, Germany)) for more than 2 days.

Polarizing microscope (Nikon, ECLIPSE LV100 N POL) is used to characterize the anisotropy of hydrogels. The optical microscope images of hydrogel and the corresponding dark and bright images in different directions (by rotating the object stage) were identified under crossed nicols.

The mechanical characterization of hydrogel is realized by using tensile machine (Electronic universal testing machine, SUNS, UMT4103). Hydrogel samples are cut into dumbbell shape, 30 mm in length, 5 mm in width, 2 mm in thickness. Both ends of the dumbbell-shaped sample were connected to the clamps with the lower clamp fixed. The upper clamp is pulled by the load cell at a constant velocity of 20 mm/min at room temperature, by which the stress–strain curve was recorded and the experimental data was further analyzed. The tensile strength is obtained from the failure point. The modulus is determined by the average slope over 0–10% of strain ratio detected from the stress-strain curve.

We use X-Ray small angle diffraction (Xeuss 2.0) to characterize the orientation structure of clay nanosheets in hydrogels. The SAXS experiments are performed at the two-dimensional SAXS instrument with the sample-to-detector was 2 m. The measuring time for each sample (20 mm in length, 7 mm in width and 2 mm in thickness) was 40 min.

3. Results and discussion

3.1. Structure of polymer networks

Poly (N-isopropylacrylamide) (PNIPAm) is a well-known particular type of polymer. It is water soluble at ambient temperatures but coagulates to become insoluble when heating at a temperature above ~32 °C, this transition is fully thermoreversible and known as the lower critical solution temperature (LCST) phenomenon [25]. Herein, PNIPAm is used to construct the first network of SC-hydrogel. Fig. 1a shows the monomers and crosslinkers used in this work. First, the PNIPAm hydrogel is prepared via radical polymerization at room temperature (Fig. 1b), using diethoxyacetophenone (DEOP) and clay nanosheets (XLS) as photo-initiator and crosslinker, respectively [26]. The utilization of clay nanosheets as crosslinker endows PNIPAm hydrogel with better elasticity, which makes a large deformation of PNIPAm hydrogel can be achieved. Second, as shown in Fig. 1c, the as-prepared clay-PNIPAm hydrogel is stretched to a certain length (150%–400%) and fixed on a glass slide, then the prestretched clay-PNIPAm hydrogel is immersed in an aqueous solution contains acrylamide, N, N′-Methylenebisacrylamide (BIS) and DEOP for a certain time (Fig. 1e). After that, we use ultraviolet light to initiate the polymerization of the secondary polyacrylamide network, thus the stretching state of clay-PNIPAm hydrogel is locked and the anisotropic double-network hydrogel is fabricated (Fig. 1f). The resultant hydrogel named as secondary crosslinked hydrogel (SC-hydrogel) with water content up to ~ 86.5%. It is worth to note that clay nanosheets were oriented along with the stretching process as illustrated in Fig. 1c. However, the orientation of clay nanosheets is changed during the swelling process of prestretched clay-PNIPAm hydrogel in acrylamide aqueous solution as shown in Fig. 1d. Detailed orientation structure of clay nanosheets in prestretched hydrogel and SC-hydrogel is further characterized by small angle X-ray scattering (SAXS) measurements, which will discussed later in this work (Fig. 4).

It is supposed that stretching the clay-PNIPAm hydrogel can induce a linear remodeling of the internal polymer networks, and the reorganized polymer networks can be substantially fixed by the secondary crosslinking of polyacrylamide chains, even after removal of the stretching force. Fig. 2a shows the photographs of hydrogels during the preparation of SC-hydrogel in different stages. The final length of SC-hydrogel (L_3 ~ 213%) after removing the mechanical force is shorter than the prestretched length (L_2 ~ 350%), but still longer than its original length (L_1 ~ 100%). These results indicate that the prestretched polymer networks of PNIPAm-hydrogel can be fixed to a certain strain by the secondary networks. The microscopic morphologies of hydrogels corresponding to that in Fig. 2a are characterized by environmental scanning electron microscopy (ESEM). The microscopic morphology of pristine clay-PNIPAm hydrogel is isotropic porous structure with a pore size about 8.8 ± 3.7 μm as shown in Fig. 2b. While, obvious oriented

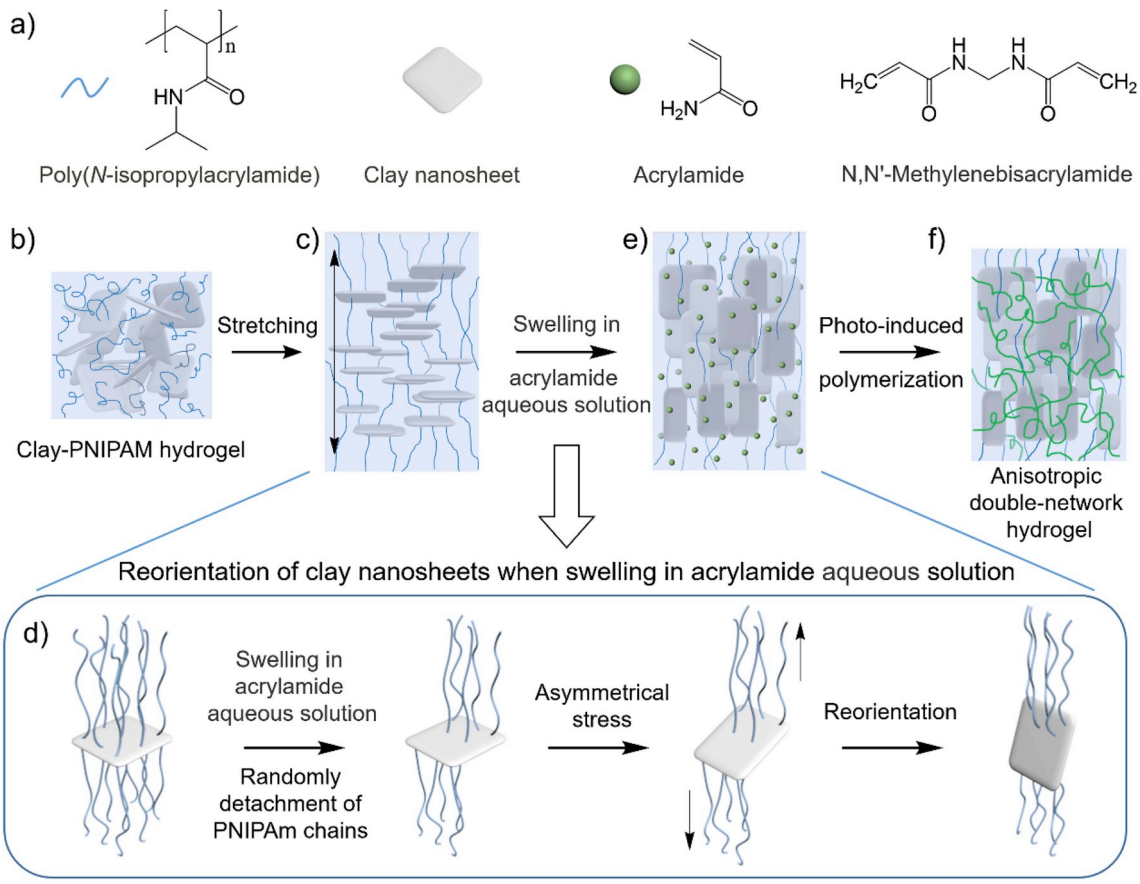

Fig. 1. Schematic illustration of the preparation of anisotropic thermoresponsive hydrogel. a) Monomers and crosslinkers used in this work. **b)** Clay-PNIPAm hydrogel is prepared by free radical polymerization. **c)** the as-prepared clay-PNIPAm hydrogel is prestretched to a certain degree. **d)** Schematic illustration shows the reorientation of clay nanosheets in prestretched clay-PNIPAm hydrogel when swelling in acrylamide aqueous solution. **e)** The swollen state of prestretched clay-PNIPAm hydrogel. **f)** The anisotropic double network hydrogel is fabricated through photo-induced polymerization of acrylamide monomers.

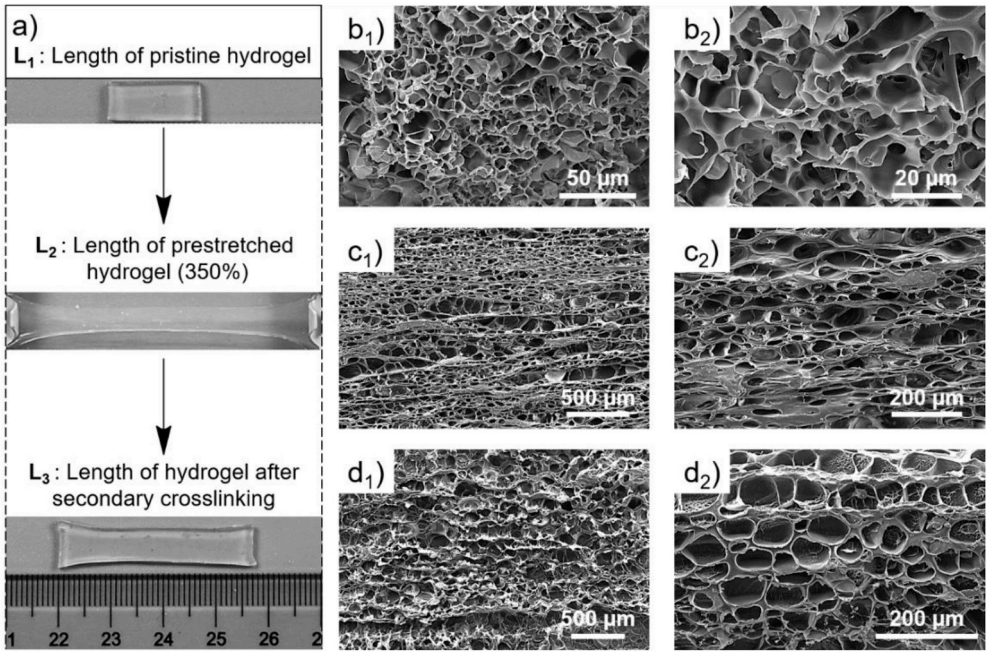

Fig. 2. Photographs and microscopic images of hydrogel in different stages during the preparation. a) Photographs of three states during the preparation of anisotropic thermoresponsive hydrogel. ESEM images show the microscopic morphology of hydrogel networks corresponding to the three states in **a). b_1-b_2)** ESEM images of pristine clay-PNIPAm hydrogel. **c1-c2)** ESEM images of prestretched clay-PNIPAm hydrogel. **d1-d2)** ESEM images of secondary crosslinked hydrogel.

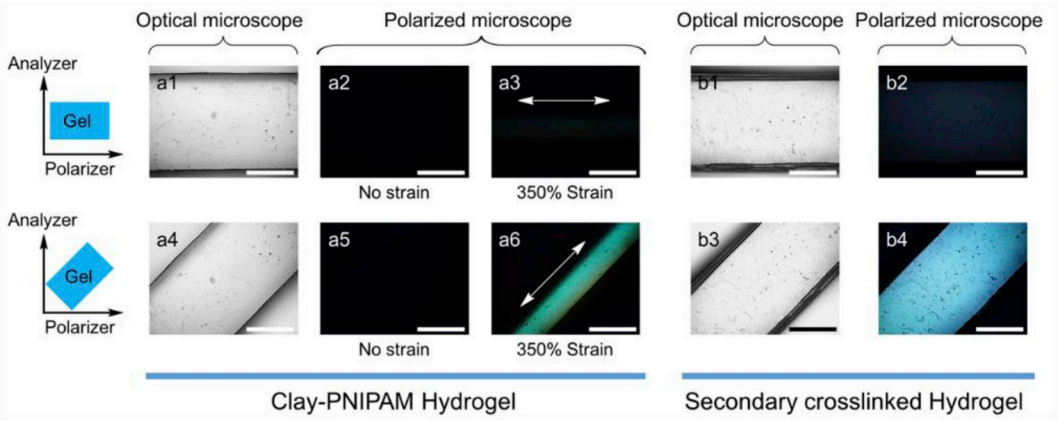

Fig. 3. Optical and polarized microscope images. a1-a6) Optical and polarized microscope images of clay-PNIPAm hydrogel with and without strain (350%). **b1-b4)**, Optical and polarized microscope images of SC-hydrogel.

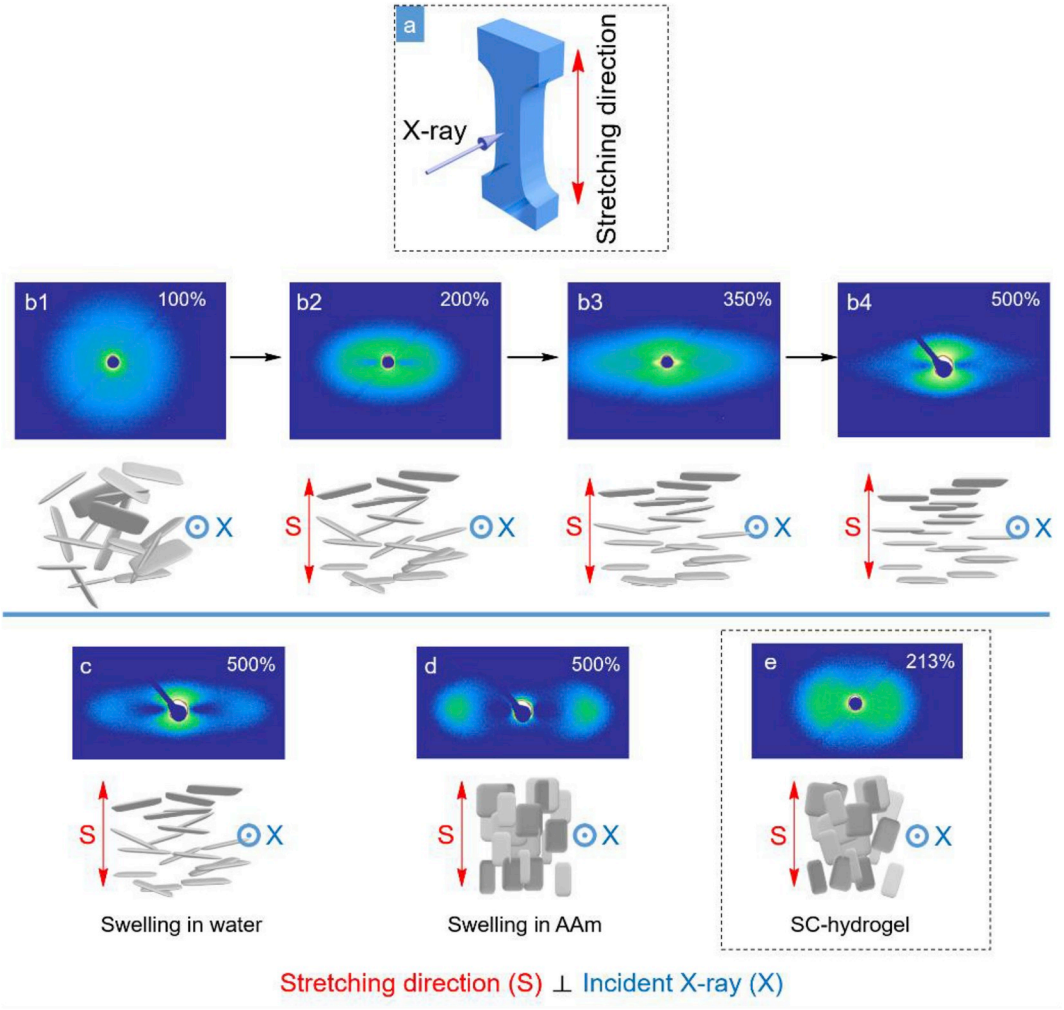

Fig. 4. 2D SAXS images of clay-PNIPAm hydrogel in different states. a) Schematic illustration shows the hydrogels are exposed to an X-ray beam from the orthogonal direction to the stretching direction. **b1-b4**) 2D SAXS images of clay-PNIPAm hydrogel under different straining ratio. **c)** 2D SAXS image of prestretched clay-PNIPAm hydrogel after swelling in water for 10 min. **d)** 2D SAXS image of prestretched clay-PNIPAm hydrogel after swelling in acrylamide aqueous solution for 10 min. **e)** 2D SAXS image of SC-hydrogel.

porous structure along the stretching direction (horizontal direction) is observed in prestretched clay-PNIPAm hydrogel (Fig. 2c). In contrast, the microscopic morphology of SC-hydrogel in Fig. 2d shows weaker orientation, which is consistent with the photographs in Fig. 2a ($L_3 < L_2$). Besides, a hierarchical porous structure is generated in SC-hydrogel, the secondary polyacrylamide network embedded in the elongated porous structure (66.7 ± 11.9 μm) of prestretched PNIPAm network is observed as shown in Fig. 2d_2. Consequently, it is supposed that the

secondary polymer networks work as fillers in SC-hydrogel and contribute to the remolding of prestretched state of clay-PNIPAm hydrogel by dissipate part of the contractile energy [27,28].

3.2. Optimized condition and anisotropy of SC-hydrogel

To investigate the optimized condition for the preparation of SC-hydrogel, a variable control method is used. For the first clay-PNIPAm hydrogel network, the ratio is fixed at 1.5 mol/L NIPAm and 10 wt% clay. The optimal prestretching ratio and swelling time is demonstrated 350% and 15 min, respectively. For the secondary polymer network, the optimal condition is demonstrated 0.5 mol/L AAm and 15 wt% BIS (Fig. S1). Then, the anisotropy of hydrogels is first characterized by polarized optical microscopy (POM). Hydrogel samples are placed at two different angle between analyzer and polarizer. As shown in Fig. 3, under crossed nicols, complete extinction is observed for pristine clay-PNIPAm hydrogel, indicates the isotropy structure of clay-PNIPAm hydrogel. While, after stretching clay-PNIPAm hydrogel to a certain extent (350%), although extinction can also be observed at the angle of analyzer-to-stretching direction = 0° (Fig. 3 a5), but obvious birefringence (maximum brightness) is observed at the angle of analyzer-to-stretching direction = 45° due to the anisotropic diffraction (Fig. 3 a6), indicates the generation of ordered structure along with the stretching process. Similarly, for SC-hydrogel, the corresponding dark and bright images at 0° and 45° directions are identified under crossed nicols as shown in Fig. 3 **b2 and b4.** Suggest that the oriented structure is preserved in SC-hydrogel. Nevertheless, because of the orientation of polymer networks and clay nanosheets in stretched hydrogel can both lead to the birefringence under crossed nicols, thus it is still uncertain whether the clay nanosheets are oriented along with the stretching process or not.

3.3. Oriented structure of clay nanosheets

To better understand the orientation of clay nanosheets during the stretching and swelling process, small angle X-ray scattering (SAXS) measurements are carried out. Schematic illustration (Fig. 4a) shows the hydrogel sample is exposed to an X-ray beam from the orthogonal to the stretching direction. The resultant 2D patterns of SAXS measurement on clay-PNIPAm hydrogel with different strain are given as shown in Fig. 4b. In the pristine clay-PNIPAm hydrogel, clay nanosheets are randomly distributed, to which PNIPAm chains are anchored. Stretching the clay-PNIPAm hydrogel, clay nanosheets gradually become oriented perpendicular to the stretching direction, giving rise to a strong scattering in the stretching direction. Further stretching the clay-PNIPAm hydrogel to 500% of its original length, the two-lobe pattern along the stretching direction become explicit as shown in Fig. 4b_4 [29]. It is worth pointing out that in spite of the increase in crosslinking inhomogeneities of hydrogel (by stretching) will contribute to the formation of "abnormal-butterfly pattern" [30], the strong scattering along the stretching direction is mainly due to the orientation of clay nanosheets. Subsequently, the orientation of clay nanosheets in prestretched clay-PNIPAm hydrogel after socking in water and aqueous solution of AAm (2 mol/L, for 10 min) were studied. As shown in Fig. 4c, scattering in stretching direction is decreased after socking in water for 10 min, while weak scattering in perpendicular to the stretching direction is emerged. The change of 2D pattern in Fig. 4c can be explained by the decrease in orientation of clay nanosheets due to the volume increase of the hydrogel by swelling. Besides, the detachment of a small fraction of PNIPAm chains (in highly tensile state) from clay nanosheets will also lead to the decrease in orientation of clay nanosheets. In contrast, a completely different 2D pattern of stretched clay-PNIPAm hydrogel is observed after socking in AAm for 10 min. As shown in Fig. 4d, scattering along stretching direction is disappeared, instead emerged in its perpendicular direction. Suggest that the reorientation of clay nanosheets in clay-PNIPAm hydrogel after swelling in AAm solution. This phenomenon is possibly ascribe to the randomly detachment of PNIPAm chains from clay nanosheets, which will further cause tension unbalance on clay platelets under internal tensile stress of oriented PNIPAm networks, resulting in the reorientation of clay nanosheets (Fig. 1c). The detachment of PNIPAm chains from clay nanosheets can be explain as follow. It is known that the initiation in clay-PNIPAm system only occurs on the clay surface and all polymer chains are attached to clay platelets through ionic or polar interactions [31]. Consequently, when hydrogel network is swollen by AAm, a portion of PNIPAm chains that attached to clay surfaces will be randomly replaced by AAm due to the stronger molecular polarity (compared with NIPAm) and high concentration of AAm monomers in the swollen hydrogel network.

The 2D pattern of SAXS measurements on SC-hydrogel is also characterized as shown in Fig. 4e, in which the scattering is perpendicular to the stretching direction but weaker than that in Fig. S4e (300% prestretching). Indicates the orientation of clay nanosheets in SC-hydrogel is preserved to a certain extent by the secondary crosslinking of polyacrylamide. The structural length between the clays can also achieved base on the SAXS data. As shown in Fig. S5, the deviations at low q region may result from destructive interference between platelets, which gives rise to a broad peak at $q \approx 0.02$ Å^{-1}. Hence, the interparticle spacing can be estimated to be $d = 2\pi/q \approx 300$ Å. Through the comparison of the curves in Fig. S5c. It is found that the structural length between the clays is slightly increased in SC-hydrogel (from 280 Å to 310 Å), which is consistent with macroscopic volume increase of SC-hydrogel after secondary crosslinking. The 2D pattern movement toward beam center in Fig. S4f (compared with Fig. S4e) also suggest that the increase of space between the clay platelets. In stretching process, it is supposed that the interparticle spacing is increased in stretching direction, while decreased in vertical direction. Consequently, the average structural length between clays during the stretching process does not change too much (≈300 Å).

3.4. Anisotropic mechanical performance of SC-hydrogel

The orientation of PNIPAm networks and clay nanosheets also contribute to the anisotropic thermoresponsive deformation of SC-hydrogel. Schematic illustration in Fig. 5a shows the anisotropic deformation mechanism of SC-hydrogel upon heating. When heating above the LCST of PNIPAm, the resultant SC-hydrogel shrink in the prestretching direction, while barely unchanged in its vertical direction (Fig. 5b). This anisotropic deformation result in a shape change of SC-hydrogel from square to rectangle as shown in Fig. 5b. In contrast, pristine clay-PNIPAm hydrogel shows reversible isotropic volume change (9.1%) in response to temperature change (Fig. 5c). The anisotropic deformation of SC-hydrogel is mainly ascribe to the ordered structure of PNIPAm networks in SC-hydrogel. When above the LCST, PNIPAm chains in tensile state coagulate to become insoluble and more easily to shrink in the stretching direction thus leading to the anisotropic deformation of SC-hydrogel. The oriented clay nanosheets, which work as crosslinkers anchor the ends of polymer chains also contribute to the orientation of PNIPAm chains and enhance the shrinkage of SC-hydrogel in stretching direction in macroscale [26]. Furthermore, the reversibility of the anisotropic deformation of SC-hydrogel is characterized using hydrogel strip. Fig. S6 show a series of snap shot of a SC-hydrogel strip during the heating and cooling process, the hydrogel strip was quickly turned from translucent to opaque and shortened by 21.3% along the prestretching direction within 1 min heating, further increase heating time will lead to isotropic contraction of SC-hydrogel. Then, the hydrogel strip became transparent again and lengthened back to its original length after 7 min cooling in water bath. This process can be repeated at least for five times (Fig. S6c), represents the good reversibility of anisotropic thermoresponsive deformation of SC-hydrogel. By taking advantage of the anisotropic thermoresponsive deformation property of SC-hydrogel, two interesting demonstrations are carried out. As shown in Fig. 5d and e, two patterns (squared array and "IRC")

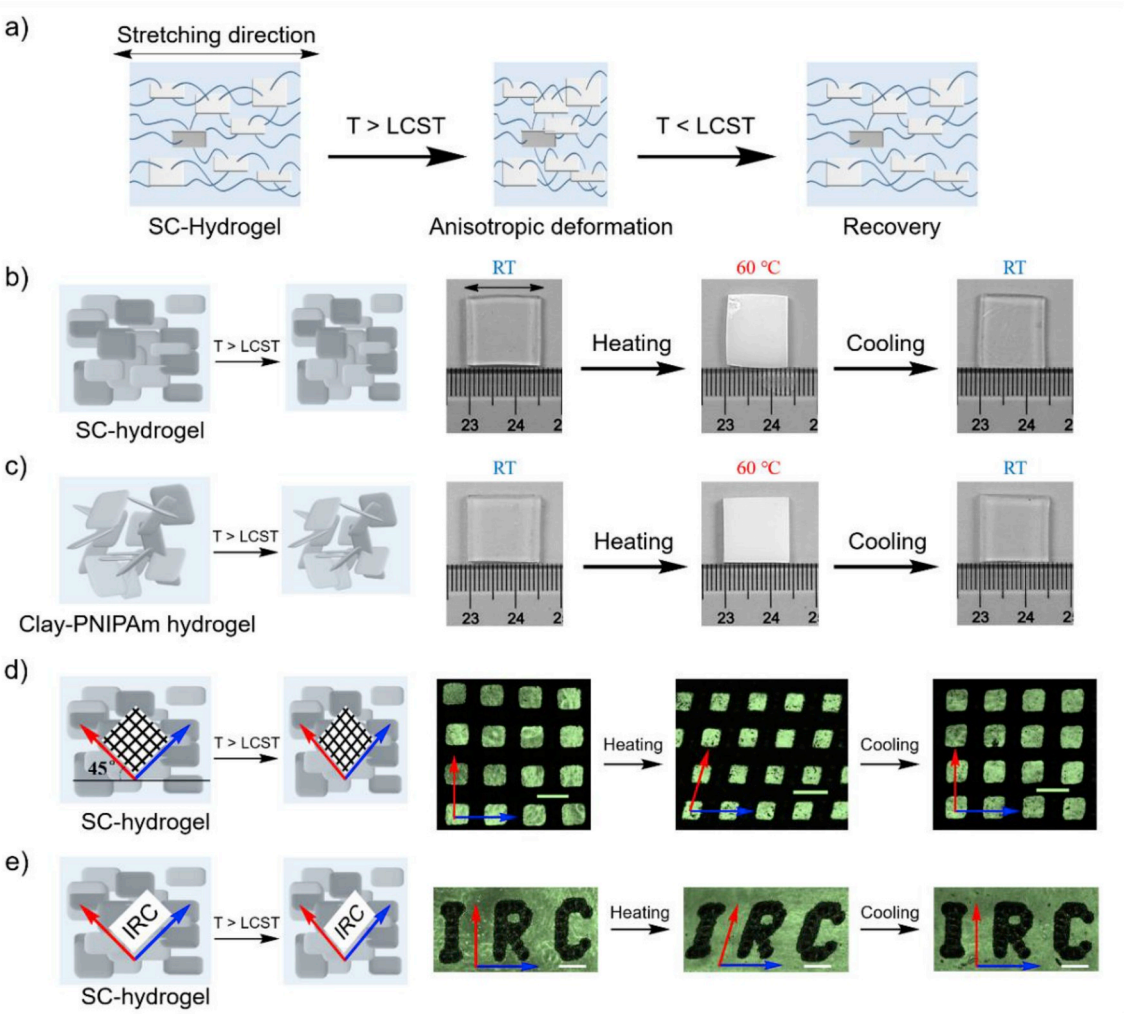

Fig. 5. Reversible anisotropic thermoresponsive deformation of SC-hydrogel. a) Schematic illustration shows the anisotropic deformation mechanism of SC-hydrogel. **b)** Anisotropic deformation of SC-hydrogel (2 mm in thickness) in response to temperature change. **c)** Isotropic volume change of pristine clay-PNIPAm hydrogel (2 mm in thickness) in response to temperature change. **d)** Reversible anisotropic thermoresponsive deformation of squared array pattern on SC-hydrogel. **e)** Reversible anisotropic thermoresponsive deformation of "IRC" pattern on SC-hydrogel (Scale bar is 500 μm).

oriented 45° to the stretching direction are prepared on SC-hydrogel surface by laser etching. As a result, the squared array turned into rhombic array with the changing of angle between two arrows from 90° to 73° by heating (above the LCST), and back to its original shape by cooling for 5 min. Similarly, the "IRC" pattern can also reversible deformed from regular capital "IRC" to italic "*IRC*" by alternately heating and cooling.

The anisotropy of SC-hydrogel also lies in the mechanical performance at two orthogonal directions (parallel and perpendicular to the prestretching direction). Tensile stress-strain curves of pristine clay-PNIPAm hydrogel and SC-hydrogel are given as shown in Fig. 6a. It is found that along the stretching direction the mechanical strength and elongation at break (90 kPa, 300%) of SC-hydrogel are obviously higher than that in its vertical direction (30 kPa, 200%), respectively. It is also found that the mechanical strength of SC-hydrogel in parallel direction is lower than the pristine clay-PNIPAm hydrogel at the beginning of the tensile test (first 100% strain). This is because of the prestretched state (L_2) during the preparation of SC-hydrogel is not totally fixed by the secondary crosslinking of polyacrylamide network, thus contracted from L_2 to L_3 (final length of as-prepared SC-hydrogel) after removal of the stretching force. Consequently, the first 100% strain of SC-hydrogel in tensile test is corresponding to the strain from L_3 to L_2, which shows lower tensile modulus compared with pristine clay-PNIPAm hydrogel. Further stretching the SC-hydrogel, the tensile modulus (slope of curves) gradually increased due to the existence of second network in SC-hydrogel. Then, the anisotropic contractile stress that generated from thermoresponsive shrinkage of SC-hydrogels is characterized. As shown in Fig. 6b, 5 times heating and cooling switch is carried out for each sample. The thermoresponsive contractile stress of SC-hydrogel in parallel direction can reach ~5 kPa. In contrast, only less than 1 kPa contractile stress is generated in vertical direction of SC-hydrogel. Finally, to show that the current SC-hydrogel is a promising candidate for artificial muscle, a load driving test is performed to characterize the load driving ability of thermoresponsive contraction of pristine clay-PNIPAm hydrogel and SC-hydrogel ($36 \times 20 \times 2$ mm^3). As shown in Fig. 6c, the thermoresponsive contraction of SC-hydrogel in parallel direction can lifting a 20 g load (18.4 times its own weight) by 18.8%. For isotropic clay-PNIPAm hydrogel, the 20 g load only lift by 9.3% (Fig. 6d). While in vertical direction, the thermoresponsive contraction of SC-hydrogel can barely lifting a 20 g load by 1% (Fig. 6e). These results demonstrate the anisotropic load driving ability of SC-hydrogel in two orthogonal directions.

4. Conclusions

In summary, to imitate the well-defined hierarchical structures

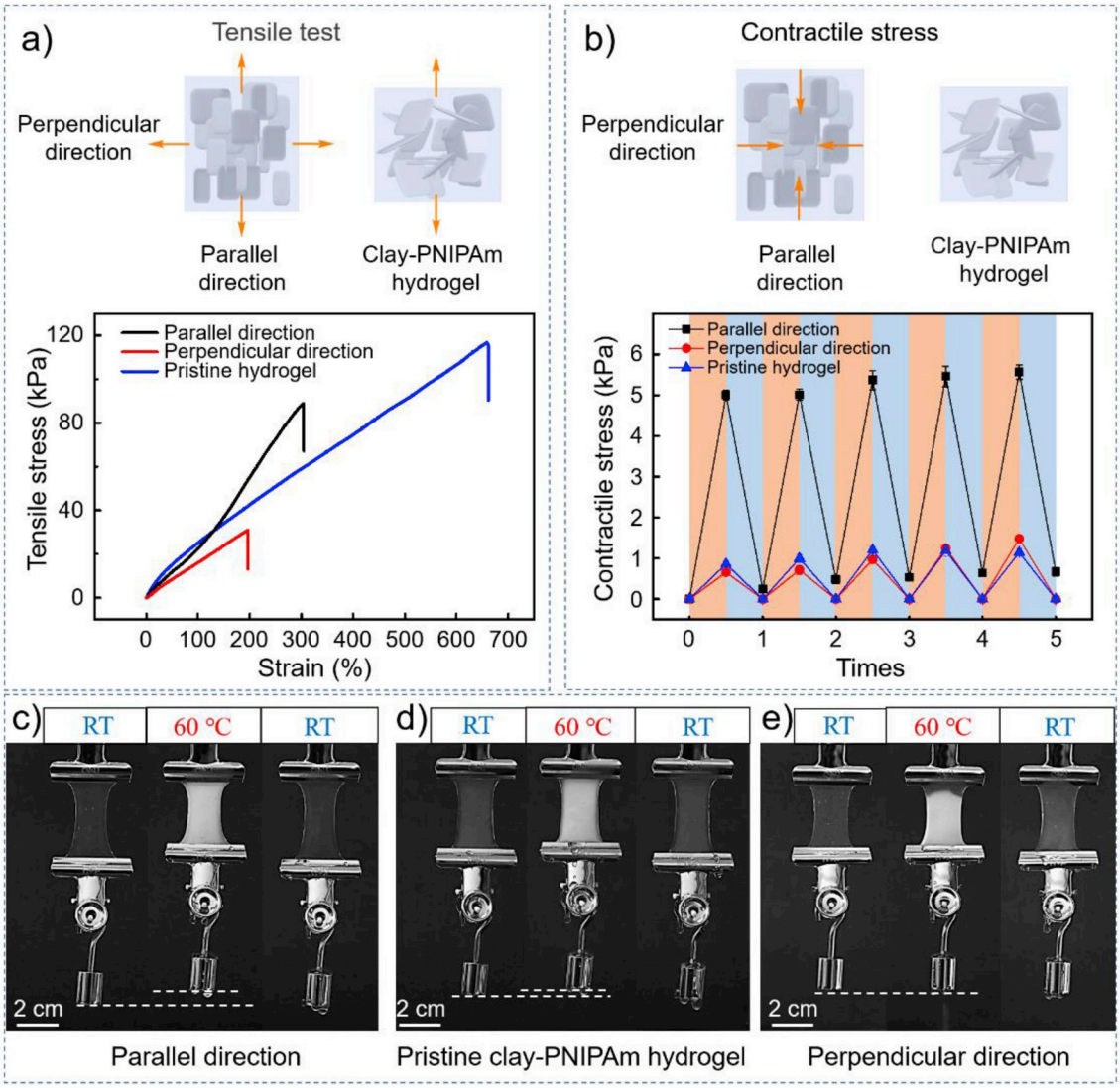

Fig. 6. Anisotropic mechanical performance of SC-hydrogel. a) Tensile stress-strain curves of clay-PNIPAm hydrogel and SC-hydrogel in perpendicular and parallel directions. **b)** Contractile stress generated from the shrinkage of single network clay-PNIPAm hydrogel and SC-hydrogel when temperature above the LCST of PNIPAm. **c)** The thermoresponsive contraction of SC-hydrogel in parallel direction can lifting a 20 g load by 18.8%. **d)** The thermoresponsive contraction of pristine clay-PNIPAm hydrogel can lifting a 20 g load by 9.3%. **e)** The thermoresponsive contraction in perpendicular direction of SC-hydrogel cannot lifting a 20 g load by 1%.

ranging from the molecular scale to macroscopic scale like biological soft tissues in hydrogels, a linear remolding of highly stretchable clay-PNIPAm nanocomposite hydrogel by a secondary crosslinking is utilized. Through this strategy, the anisotropic thermoresponsive hydrogels are fabricated. The as-prepared SC-hydrogel exhibits reversible anisotropic thermoresponsive property. Subsequently, the oriented structures of polymer network and clay nanosheets in hydrogel are carefully studied and discussed. Moreover, the SC-hydrogel also shows anisotropic mechanical performance. Taking advantage of this property, the anisotropic thermoresponsive load driving is realized base on SC-hydrogel. Consequently, it is supposed that the as-prepared SC-hydrogel closely mimic the natural actuator "skeletal muscle", not only in composition, but also structurally and functionally. The special functions of current SC-hydrogel also suggest that it may serve as ideal composite gel materials with validity in a variety of applications, such as soft actuators, sensors, and biological materials.

Declaration of competing interest

The authors declare that they have no known competing financial interests or personal relationships that could have appeared to influence the work reported in this paper.

CRediT authorship contribution statement

Lie Chen: Conceptualization, Methodology, Data curation, Writing - original draft, Formal analysis, Software. **Qingshan Wu:** Data curation, Writing - original draft. **Jianqi Zhang:** Formal analysis, Software. **Tianyi Zhao:** Supervision, Investigation. **Xu Jin:** Validation. **Mingjie Liu:** Conceptualization, Methodology, Supervision, Investigation, Writing - review & editing.

Acknowledgements

L. Chen and Q. Wu contributed equally to this work. This work was financially supported by the National Key R&D Program of China (Grant

2017YFA0207800), the National Natural Science Funds for Distinguished Young Scholar (No. 21725401), and the China Postdoctoral Science Foundation (2019M650434).

Appendix A. Supplementary data

Supplementary data to this article can be found online at https://doi.org/10.1016/j.polymer.2020.122309.

References

[1] Z. Zhao, R. Fang, Q. Rong, M. Liu, Bioinspired nanocomposite hydrogels with highly ordered structures, Adv Mater 29 (45) (2017).
[2] X. Le, W. Lu, J. Zhang, T. Chen, Recent progress in biomimetic anisotropic hydrogel actuators, Adv. Sci. 6 (5) (2019) 1801584.
[3] M.A. Geeves, Molecular motors: stretching the lever-arm theory, Nature 415 (6868) (2002) 129–131.
[4] K. Oliver, A. Seddon, R.S. Trask, Morphing in nature and beyond: a review of natural and synthetic shape-changing materials and mechanisms, J. Mater. Sci. 51 (24) (2016) 10663–10689.
[5] S. Choi, J. Kim, Designed fabrication of super-stiff hybrid hydrogel via linear remodeling of polymer networks and subsequent crosslinking, J. Mater. Chem. B 3 (8) (2015) 1479–1483.
[6] P. Lin, T. Zhang, X. Wang, B. Yu, F. Zhou, Freezing molecular orientation under stretch for high mechanical strength but anisotropic hydrogels, Small 12 (32) (2016) 4386–4392.
[7] M.A. Haque, G. Kamita, T. Kurokawa, K. Tsujii, J.P. Gong, Unidirectional alignment of lamellar bilayer in hydrogel: one-dimensional swelling, anisotropic modulus, and stress/strain tunable structural color, Adv Mater 22 (45) (2010) 5110–5114.
[8] D. Ye, Q. Cheng, Q. Zhang, Y. Wang, C. Chang, L. Li, H. Peng, L. Zhang, Deformation drives alignment of nanofibers in framework for inducing anisotropic cellulose hydrogels with high toughness, ACS Appl. Mater. Interfaces 9 (49) (2017) 43154–43162.
[9] A.L. Buyanov, I.V. Gofman, L.G. Revel'Skaya, A.K. Khripunov, A.A. Tkachenko, Anisotropic swelling and mechanical behavior of composite bacterial cellulose–poly(acrylamide or acrylamide–sodium acrylate) hydrogels, Journal of the Mechanical Behavior of Biomedical Materials 3 (1) (2010) 102–111.
[10] T. Zhao, G. Wang, D. Hao, L. Chen, K. Liu, M. Liu, Macroscopic layered organogel-hydrogel hybrids with controllable wetting and swelling performance, Adv. Funct. Mater. 28 (49) (2018) 1800793.
[11] L. Maggini, M. Liu, Y. Ishida, D. Bonifazi, Anisotropically luminescent hydrogels containing magnetically-aligned MWCNTs-Eu(III) hybrids, Adv Mater 25 (17) (2013) 2462–2467.
[12] K. Murata, K. Haraguchi, Optical anisotropy in polymer–clay nanocomposite hydrogel and its change on uniaxial deformation, J. Mater. Chem. 17 (32) (2007) 3385.
[13] Y. Takashima, S. Hatanaka, M. Otsubo, M. Nakahata, T. Kakuta, A. Hashidzume, H. Yamaguchi, A. Harada, Expansion-contraction of photoresponsive artificial muscle regulated by host-guest interactions, Nat. Commun. 3 (2012) 1270.
[14] Y.S. Kim, M. Liu, Y. Ishida, Y. Ebina, M. Osada, T. Sasaki, T. Hikima, M. Takata, T. Aida, Thermoresponsive actuation enabled by permittivity switching in an electrostatically anisotropic hydrogel, Nat. Mater. 14 (10) (2015) 1002–1007.
[15] S. Ahadian, J. Ramon-Azcon, M. Estili, X. Liang, S. Ostrovidov, H. Shiku, M. Ramalingam, K. Nakajima, Y. Sakka, H. Bae, T. Matsue, A. Khademhosseini, Hybrid hydrogels containing vertically aligned carbon nanotubes with anisotropic electrical conductivity for muscle myofiber fabrication, Sci. Rep. 4 (2014) 4271.
[16] B. Lu, H. Yuk, S. Lin, N. Jian, K. Qu, J. Xu, X. Zhao, Pure PEDOT:PSS hydrogels, Nat. Commun. 10 (1) (2019) 1043.
[17] M. Liu, Y. Ishida, Y. Ebina, T. Sasaki, T. Hikima, M. Takata, T. Aida, An anisotropic hydrogel with electrostatic repulsion between cofacially aligned nanosheets, Nature 517 (7532) (2015) 68–72.
[18] W. Linlin, O. Masataka, T. Masaki, S. Akinori, S. Shu, I. Yasuhiro, A. Takuzo, Magnetically induced anisotropic orientation of graphene oxide locked by in situ hydrogelation, ACS Nano 8 (5) (2014) 4640.
[19] M.A. Haque, T. Kurokawa, J.P. Gong, Anisotropic hydrogel based on bilayers: color, strength, toughness, and fatigue resistance, Soft Matter 8 (31) (2012) 8008.
[20] W. Yang, H. Furukawa, J.P. Gong, Highly extensible double-network gels with self-assembling anisotropic structure, Adv. Mater. 20 (23) (2008) 4499–4503.
[21] G. Schmidt, A.I. Nakatani, P.D. Butler, C.C. Han, Small-angle neutron scattering from viscoelastic polymer-clay solutions, Macromolecules 35 (12) (2002) 4725–4732.
[22] L. Sardone, V. Palermo, E. Devaux, D. Credgington, M. de Loos, G. Marletta, F. Cacialli, J. van Esch, P. Samorì, Electric-field-assisted alignment of supramolecular fibers, Adv. Mater. 18 (10) (2006) 1276–1280.
[23] L. Liu, S. Jiang, Y. Sun, S. Agarwal, Giving direction to motion and surface with ultra-fast speed using oriented hydrogel fibers, Adv. Funct. Mater. 26 (7) (2016) 1021–1027.
[24] I. Kundler, H. Finkelmann, Strain-induced director reorientation in nematic liquid single crystal elastomers, Macromol. Rapid Commun. 16 (9) (2010).
[25] H.G. Schild, Poly(N -isopropylacrylamide): experiment, theory and application, Prog. Polym. Sci. 17 (2) (1992) 163–249.
[26] K. Haraguchi, H.J. Li, Mechanical properties and structure of Polymer−Clay nanocomposite gels with high clay content, Macromolecules 39 (5) (2006) 1898–1905.
[27] J.P. Gong, Y. Katsuyama, T. Kurokawa, Y. Osada, Double-network hydrogels with extremely high mechanical strength, Adv. Mater. 15 (14) (2003) 1155–1158.
[28] J.P. Gong, Why are double network hydrogels so tough? Soft Matter 6 (12) (2010) 2583–2590.
[29] Mitsuhiro Shibayama, Takeshi Karino, Sho Miyazaki, Satoshi Okabe, A. Toru Takehisa, K. Haraguchi, Small-angle neutron scattering study on uniaxially stretched poly(N-isopropylacrylamide)−Clay nanocomposite gels, Macromolecules 38 (26) (2005) 10772–10781.
[30] E. Mendes, R. Oeser, C. Hayes, F. Boué, J. Bastide, Small-angle neutron scattering study of swollen elongated gels: butterfly patterns, Macromolecules 29 (17) (1996) 5574–5584.
[31] K. Haraguchi, H.-J. Li, K. Matsuda, T. Takehisa, E. Elliott, Mechanism of forming organic/inorganic network structures during in-situ free-radical polymerization in PNIPA−Clay nanocomposite hydrogels, Macromolecules 38 (8) (2005) 3482–3490.